Neuron, Vol. 31, 289–303, August 2, 2001, Copyright ©2001 by Cell Press

Regulation of Dendritic Spine Morphology by SPAR, a PSD-95-Associated RapGAP

Daniel T.S. Pak,[1,4] Soyoung Yang,[2] Sheila Rudolph-Correia,[1] Eunjoon Kim,[2] and Morgan Sheng[1,3,4]
[1] Department of Neurobiology and Howard Hughes Medical Institute Massachusetts General Hospital and Harvard Medical School Boston, Massachusetts 02114
[2] Department of Biological Sciences Korea Advanced Institute for Science and Technology Taejon 305-701 Korea

Summary

The PSD-95/SAP90 family of scaffold proteins organizes the postsynaptic density (PSD) and regulates NMDA receptor signaling at excitatory synapses. We report that SPAR, a Rap-specific GTPase-activating protein (RapGAP), interacts with the guanylate kinase-like domain of PSD-95 and forms a complex with PSD-95 and NMDA receptors in brain. In heterologous cells, SPAR reorganizes the actin cytoskeleton and recruits PSD-95 to F-actin. In hippocampal neurons, SPAR localizes to dendritic spines and causes enlargement of spine heads, many of which adopt an irregular appearance with putative multiple synapses. Dominant negative SPAR constructs cause narrowing and elongation of spines. The effects of SPAR on spine morphology depend on the RapGAP and actin-interacting domains, implicating Rap signaling in the regulation of postsynaptic structure.

Introduction

Spines are small protrusions on dendritic shafts that constitute the primary loci of excitatory synaptic transmission in the mammalian CNS. Dendritic spines are heterogeneous in shape, and their density and morphology are influenced by many factors, including age, hormones, neurotrophins, learning, and synaptic activity (Horner, 1993; Harris and Kater, 1994). The plasticity of spine structure may contribute to long-term memory storage (Crick, 1982; Bailey and Kandel, 1993). Indeed, stimuli that induce long-term potentiation (LTP) have been associated with altered spine size (Fifkova and Van Harreveld, 1977; Chang and Greenough, 1984), increased synaptic surface area (Desmond and Levy, 1988), and perforation of the postsynaptic density (Toni et al., 1999). The molecular mechanisms that regulate the size and shape of dendritic spines are poorly understood.

The actin cytoskeleton is a likely target of the molecular mechanisms regulating spine morphology (reviewed in Matus, 2000). Spines are actin-rich and undergo rapid, actin-dependent motility (Fischer et al., 1998). The structure of dendritic spines and F-actin is influenced by glutamate receptor activity (Segal, 1995; Halpain et al., 1998; McKinney et al., 1999), and LTP-inducing stimuli can promote new spine formation via NMDA receptor-dependent mechanisms (Engert and Bonhoeffer, 1999; Maletic-Savatic et al., 1999).

What are the signaling pathways that link glutamate receptor activity to the postsynaptic actin cytoskeleton? Glutamate receptors interact directly or indirectly with actin binding proteins and regulators of the actin cytoskeleton. For example, the actin binding protein α-actinin binds directly to NMDA receptors (Wyszynski et al., 1997). In addition, PSD-95/SAP90 family proteins function as molecular adaptors between glutamate receptors and intracellular signaling and cytoskeletal networks. PSD-95 is a major component of PSDs (Cho et al., 1992; Kistner et al., 1993) and is characterized by three N-terminal PDZ domains, an SH3 domain, and a C-terminal guanylate kinase-like (GK) domain, all of which function as modular protein interaction domains. For example, the first two PDZ domains of PSD-95 interact with the C termini of NMDA receptor NR2 subunits (Kornau et al., 1995; Niethammer et al., 1996), whereas all three PDZ domains bind to the C terminus of SynGAP, a GTPase activating protein (GAP) for Ras (Chen et al., 1998; Kim et al., 1998).

The Rap family of small GTPases is closely related to Ras, and contains two members, Rap1 and Rap2 (Zwartkruis and Bos, 1999). The cellular functions of Rap proteins are unclear; various roles have been described in different cell types, including regulation of Raf/MAP kinase cascades (Vossler et al., 1997; but see Zwartkruis et al., 1998), establishment and maintenance of cell adhesion (Tsukamoto et al., 1999), and activation of integrins (Caron et al., 2000; Reedquist et al., 2000). In yeast, a Rap homolog (BUD1) is required for budding and recruits factors for polarized organization of the actin cytoskeleton (Cabib et al., 1998). Thus, mounting evidence suggests a role for Rap in the regulation of actin cytoskeleton and cell-cell or cell-matrix interactions. Several Rap-specific activators, or GEFs (guanine nucleotide exchange factors) have been identified. Of particular interest is nRapGEP, a neural-specific GEF that can interact with the synaptic scaffold protein, S-SCAM (Ohtsuka et al., 1999). However, little is known about the function of Rap in neurons or synapses.

We now report that a GAP for Rap (termed SPAR, for Spine-associated RapGAP) binds to the GK domain of PSD-95. SPAR has actin-reorganizing activity, targets to dendritic spines of neurons, and regulates spine morphology via its GAP and actin-interacting domains.

Results

SPAR Interacts with the GK Domain of PSD-95

We conducted a yeast two-hybrid screen of a rat brain cDNA library, using as bait the C-terminal region of chap-

[3] Correspondence: msheng@mit.edu
[4] Present address: Center for Learning and Memory, Massachusetts Institute of Technology, Cambridge, Massachusetts 02139.

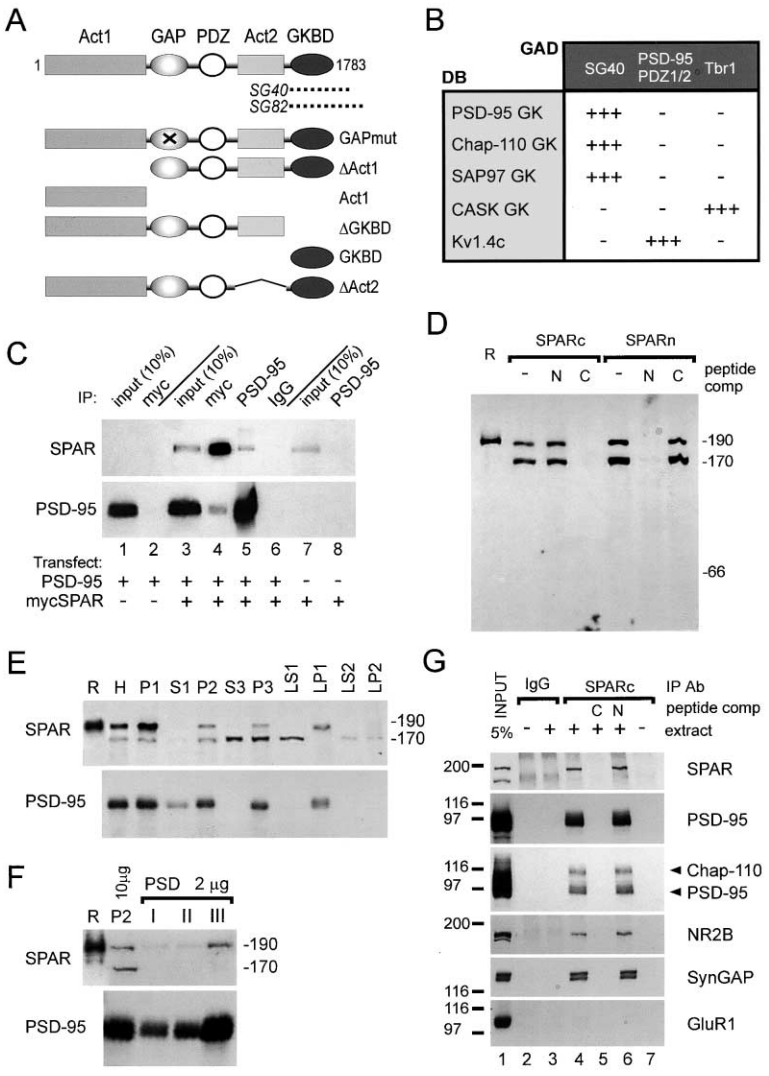

Figure 1. Interaction of SPAR and PSD-95

(A) Domain organization of SPAR and constructs used in this study. SG40 and SG82 are independent cDNA clones isolated from a yeast two-hybrid screen using as bait the SH3 and GK domains of chapsyn-110/PSD-93.

(B) Interaction of SPAR and PSD-95 in yeast two-hybrid system. SG40, containing the C-terminal 278 amino acids of SPAR fused to the GAL4 activation domain (GAD) interacts with LexA DNA binding domain (DB) fusions of the GK domain of PSD-95, chapsyn-110, and SAP97, but not with the GK domain of CASK or the C-terminal tail of Kv1.4. Tbr1 and PDZ 1/2 of PSD-95 are positive controls for the GK of CASK and the C terminus of Kv1.4, respectively. +++, 0–30 min β-gal detection time. −, no detectable β-gal signal after 12 hr.

(C) Coimmunoprecipitation of SPAR and PSD-95 from COS-7 cells. Extracts of COS-7 cells transfected with myc-SPAR, PSD-95, or both, as indicated, were immunoprecipitated with myc or PSD-95 antibodies or nonimmune IgG. Precipitates were immunoblotted for PSD-95 and myc. Input represents 10% of the lysate used for the immunoprecipitation reaction.

(D) Immunoblots of adult rat brain homogenates using SPARc and SPARn antibodies. The upper 190 kDa band (SPAR-190) comigrates with full-length SPAR expressed in COS-7 cells (lane R). SPARc and SPARn signals are specifically eliminated by competition with the respective antigenic peptide.

(E) Subcellular fractionation of SPAR and PSD-95 in rat brain. R, recombinant SPAR expressed in COS cells. H, total homogenate of rat brain. P2, crude synaptosome; S3, cytosol; P3, light membrane; LP1, synaptosomal membrane; LP2, synaptic vesicle fraction.

(F) Coenrichment of SPAR and PSD-95 in the PSD. Lane R, COS-7 cells transfected with SPAR cDNA. P2, crude synaptosomal membrane fraction (10 μg protein). PSD I, II, and III, postsynaptic density fractions prepared by extraction of synaptosomes once (I) or twice (II) with Triton X-100 or with Triton X-100 and sarkosyl (III) (2 μg protein).

(G) Coimmunoprecipitation of SPAR and PSD-95 from brain extracts. Deoxycholate extracts of rat brain were immunoprecipitated with nonimmune rabbit IgG or affinity purified SPARc antibodies, and immunoblotted for the indicated proteins. Competition with the immunogenic C-terminal peptide (lane 5), but not the unrelated N-terminal peptide (lane 6), abolished the recovery of SPAR and associated proteins. Immunoprecipitations were performed without added brain extracts in lanes 2 and 7.

syn-110/PSD-93 that contains the SH3 and GK domains (Kim et al., 1996). Most of the positive interactors were members of the GKAP/SAPAP/DAP family of proteins that bind to the GK domain of PSD-95 family proteins (Kim et al., 1997; Satoh et al., 1997; Takeuchi et al., 1997). However, two independent clones isolated in this screen (SG40 and SG82) encoded the C-terminal 278 and 277 amino acids, respectively, of a distinct protein that we named SPAR (Figure 1A). The GK domain of chapsyn-110/PSD-93 was sufficient for binding to SPAR in the yeast two-hybrid system (Figure 1B). SPAR also interacted with the GK domain of PSD-95 and SAP97/hDlg, but not with the GK domain of CASK (Hsueh et al., 2000) (Figure 1B). Deletion analysis failed to define a smaller portion of SPAR capable of binding to the GK domain of PSD-95 in the yeast two-hybrid system. Thus, the C-terminal ~280 amino acids of SPAR (termed here the GK binding domain, or GKBD) interacts specifically with the GK domain of PSD-95 family proteins.

A sequence of SPAR had been deposited in GenBank and annotated as "Spa-1-like protein" and "PSD-95 GK interactor" (accession #AF026504) (see also Deguchi et al., 1998). Over its 1783 residue length, SPAR is 95% identical to a human protein named E6TP1α previously identified as a target for degradation by human papilloma virus (HPV) E6 oncoprotein (Gao et al., 1999). Several motifs were recognized in the primary sequence of SPAR (Figure 1A), most notably a PDZ domain and a region homologous to the catalytic domain of RapGAPs such as Spa-1 (Hattori et al., 1995; Kurachi et al., 1997). The N-terminal region of SPAR upstream of the GAP domain, and a serine-rich region between the PDZ domain and the GKBD, are designated Act1 and Act2 for reasons described later.

We performed coimmunoprecipitation assays to verify the interaction of full-length SPAR and PSD-95 in mammalian cells. From COS-7 cells doubly transfected with PSD-95 and myc-tagged SPAR, anti-myc antibodies precipitated the majority of myc-SPAR and a minor fraction of PSD-95 (Figure 1C, lane 4). Myc antibodies did not precipitate PSD-95 in the absence of myc-SPAR. Conversely, anti-PSD-95 antibodies precipitated a small amount of myc-SPAR only when PSD-95 was coexpressed (Figure 1C, lane 5). Nonimmune IgGs did not precipitate either mycSPAR or PSD-95 (lane 6). A SPAR construct lacking the GKBD failed to interact with PSD-95, whereas the GKBD alone was sufficient for coimmunoprecipitation with PSD-95 in COS-7 cells (data not shown).

Association of SPAR and PSD-95 in Brain

We raised peptide antibodies against the N and C terminus of SPAR (SPARn and SPARc antibodies). Both antibodies recognized the same doublet of bands (190 and 170 kDa) on immunoblots of rat brain (Figure 1D). The 190 kDa band comigrated with recombinant SPAR expressed heterologously in COS-7 cells (Figure 1D, lane R); thus the 190 kDa band (SPAR-190) presumably corresponds to the full-length SPAR protein. The 170 kDa band (SPAR-170) likely represents an alternative splice product, although its molecular nature remains to be established.

In brain extracts, SPAR-190 showed a similar fractionation profile to PSD-95 (Figure 1E), with both proteins found primarily in membrane fractions, P2 (crude synaptosome), P3 (light membrane), and LP1 (synaptosomal membrane). Furthermore, SPAR-190 coenriched with PSD-95 during purification of PSDs (Figure 1F), being most enriched in PSDIII, a "core" PSD preparation extracted with Triton X-100 and sarkosyl detergents. SPAR-170 fractionation differed from SPAR-190; SPAR-170 was abundant in cytosolic fractions (S3) and did not copurify with the PSD (Figures 1E and 1F).

To test for a native association of SPAR and PSD-95, coimmunoprecipitation experiments were performed using whole brain lysates from adult rats (Figure 1G). SPARc antibodies precipitated SPAR–190 (Figure 1G, lane 4) but not SPAR-170. In addition, the SPARc antibodies coimmunoprecipitated PSD-95 and its close relative chapsyn-110/PSD-93, as well as NMDA receptors (NR2B) and SynGAP (Figure 1G, lane 4). AMPA receptors (GluR1) were not captured by SPARc antibodies (Figure 1G), and nonimmune rabbit IgGs failed to precipitate any of the proteins examined (Figure 1G, lane 3). Competition with the C-terminal peptide used to generate SPARc antibodies abolished the recovery of SPAR, PSD-95, and associated proteins (Figure 1G, lane 5), while the N-terminal SPAR peptide had no effect on the coimmunoprecipitation (Figure 1G, lane 6). We were unable to show coimmunoprecipitation of SPAR using anti-PSD-95 antibodies, perhaps because PSD-95 is present in great excess over SPAR. The coimmunoprecipitation data indicate that SPAR is a component of the NMDA receptor/PSD-95 protein complex.

SPAR Is a Rap-Specific GAP

Because SPAR contains a domain homologous to the GTPase-activating domains of RapGAPs, we tested the GAP activity of SPAR in vitro. Purified small GTPases H-Ras, Rap1A, and Rap2A were loaded with [^{32}P]γ-GTP and incubated with either buffer or SPAR immunoprecipitated from COS-7 lysates. In the presence of buffer alone, all three GTPases exhibited low GTPase activity, as measured by the level of bound [^{32}P]γ-GTP (Figures 2A–2C, filled triangles). The intrinsic activity of H-Ras appeared to be the highest of the GTPases tested, consistent with previous reports that the GTPase activity of Rap1 is 10-fold lower than Ras (Noda, 1993). The addition of SPAR greatly stimulated the GTPase activity of Rap, such that Rap2A hydrolyzed its bound GTP nearly to completion by 30 min (Figure 2A). Rap1A GTPase activity was also stimulated by SPAR, though to a lesser degree than Rap2A (Figure 2B). The GTPase activities of H-Ras, RhoA, Rac1, and Cdc42 were unaffected by SPAR (Figure 2C; and not shown). Immunoprecipitates from COS cells transfected with empty vector had no effect on either Rap or Ras (Figures 2A–2D, open circles).

We generated GAP domain mutants of SPAR with substitutions at various conserved residues within two "arginine fingers" common to RapGAP domains (Figure 2F) (Scheffzek et al., 1998). Most of the single point mutations decreased, but did not abolish, SPAR's GAP activity against Rap2 (e.g., R704A and R807A; Figure 2D). One double mutant, R807A/T808S (referred to later as GAPmut), was devoid of GAP activity in this assay (Figure 2D). The lack of activity was not due to reduced protein expression because all GAP domain mutants tested were expressed at comparable levels (Figure 2E). We conclude that SPAR is bona fide RapGAP that acts selectively on the Rap subfamily of GTPases.

Reorganization of F-Actin by SPAR

Because certain Rap or RapGAP proteins have been implicated in cytoskeletal regulation (Cabib et al., 1998; Torti et al., 1999; Tsukamoto et al., 1999; Boettner et al., 2000), we tested whether SPAR could affect the cytoskeleton when expressed in heterologous cells. COS-7 cells transfected with myc-tagged SPAR or with vector alone were double-labeled with myc antibodies to detect the recombinant SPAR protein and with phalloidin-rhodamine to visualize F-actin (Figure 3). Control cells transfected with vector alone showed a normal pattern of fine actin stress fibers (Figure 3A1), and no myc-staining (Figure 3A2). In contrast, the F-actin cytoskeleton in all cells transfected with myc-SPAR was dramatically reorganized, forming a variety of atypical structures that fell into three major categories: large aggregates, usually lying near the cell periphery (Figure 3B1), dispersed clusters (Figure 3C1), and smaller well-defined star-like clusters (Figure 3D1). Whatever the pattern of F-actin derangement, the distribution of myc-SPAR coincided precisely with the phalloidin staining, indicating a close association between SPAR and the reorganized F-actin (Figures 3B2, 3C2 and 3D2). The effect of SPAR appeared specific for actin, because SPAR had no discernible influence on, and did not codistribute with, microtubules (Figures 3E1–3E3 and Figure 3F).

To identify the domains of SPAR responsible for its interaction with actin, we performed a deletion analysis of SPAR in COS cells. Remarkably, two separate regions

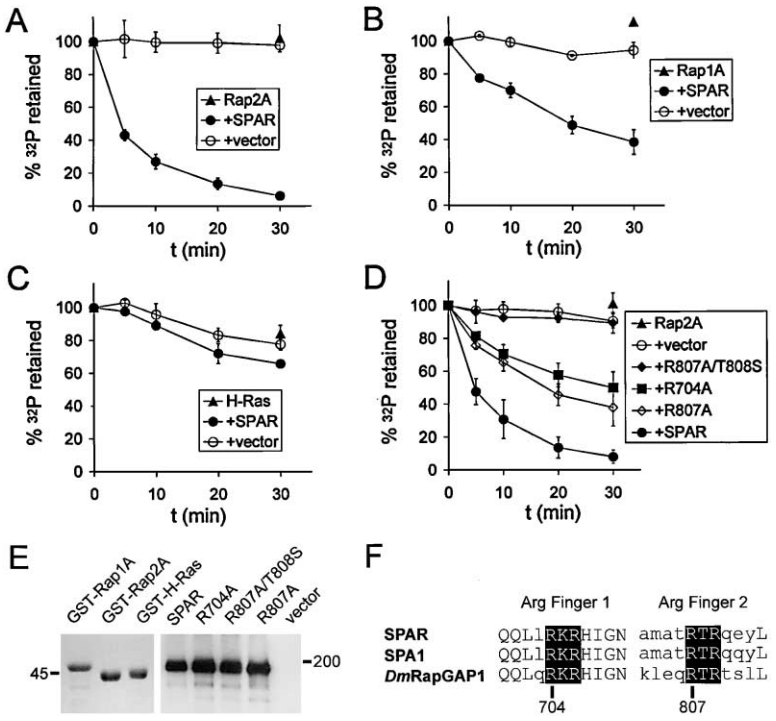

Figure 2. In Vitro Assay for GAP Activity of SPAR

(A–C) GST fusions of Rap2A (A), Rap1A (B), and H-Ras (C) were loaded with [^{32}P]γ-GTP and then incubated with buffer (filled triangles), or anti-myc immunoprecipitates from COS cells transfected with myc-SPAR (filled circles), or vector only (open circles). The amount of bound [^{32}P]γ-GTP remaining at various times was determined by filtration through nitrocellulose filters. Means $\pm$ SD are shown for at least three experiments per time course.

(D) GAP activity of SPAR mutants. Mutant R807A/T808S, which has no GAP activity, is also referred to as GAPmut.

(E) Left panel, Coomassie staining of purified GST-fusions of GTPases. Right panel, immunoblot of imunoprecipitated wild-type and mutant SPAR proteins from COS lysates demonstrating equivalent expression of each protein. Size markers in kD.

(F) Alignment of "arginine finger" motifs in representative RapGAP proteins. Absolutely conserved residues in all RapGAPs are capitalized.

of SPAR (Act1 and Act2; see Figure 1A) were independently capable of colocalizing with and reorganizing F-actin (Figures 3G and 3H). However, the effects of Act1 and Act2 were not equivalent. Act1 reproducibly caused virtually all of the F-actin in the cell to accumulate on numerous tubulovesicular structures, many of which appeared to be aggregated in clumps (Figure 3G1). Act2 induced F-actin to coalesce in thick spikes (Figure 3H1), some of which formed star-like structures akin to those observed with full-length SPAR (Figure 3D1), but on a much larger scale (Figure 3H1). Both Act1 and Act2 domains of SPAR were highly colocalized with the altered F-actin structures that they induced (Figures 3G2 and 3H2).

In COS cells, PSD-95 expressed alone was diffusely distributed and had no effect on F-actin (Figure 4A). When coexpressed with SPAR, however, PSD-95 redistributed into clusters that colocalized with SPAR (Figures 4B1 and 4B2). Clustering of PSD-95 occurred in 78% of cells cotransfected with SPAR (n = 100). Significantly, PSD-95 became colocalized with the reorganized F-actin aggregates in the presence of SPAR (Figures 4C1 and 4C2), just like SPAR itself (Figures 4D1 and 4D2). In COS cells cotransfected with SPAR and a PSD-95 mutant lacking the GK domain (PSD-95ΔGK), PSD-95ΔGK remained diffuse in the cytoplasm (Figure 4E2) while SPAR codistributed with F-actin clusters (Figure 4E1). Similarly, wild-type PSD-95 remained diffusely distributed in the cell (Figure 4F2) when coexpressed with a SPAR mutant lacking the PSD-95 binding region (ΔGKBD; Figure 4F1). ΔGKBD could still efficiently reorganize and associate with F-actin (Figures 4F1, 4H1, and 4H2), but it was unable to recruit PSD-95 to the actin clusters (Figures 4G1 and 4G2). In conclusion, SPAR is able to mediate the association of PSD-95 and F-actin in COS cells, in a manner dependent on both the GK domain of PSD-95 and the GKBD of SPAR. However, the reorganization of F-actin by SPAR does not require the GKBD, consistent with the SPAR deletion analysis shown earlier (Figures 3G and 3H).

Targeting of SPAR to Dendritic Spines

The distribution of endogenous SPAR was studied in hippocampal cultures (DIV19–21) using affinity-purified SPARn antibodies. SPAR expression was very low or undetectable in glial cells and GABAergic interneurons (data not shown). SPAR immunoreactivity was present in all spiny neurons, concentrated in dendritic clusters that colocalized with PSD-95 (Figure 5A; Figure 5B1, arrowheads) and with α-actinin, a spine-enriched actin binding protein (Figure 5B2). SPAR clusters were apposed to, rather than precisely overlapping with, the synaptic vesicle protein synaptophysin (Figure 5B3), suggesting that SPAR is predominantly postsynaptic in distribution. The numerous SPAR clusters showed no colocalization with GAD puncta (Figure 5B4), indicating that SPAR is absent from inhibitory synapses present on the dendritic shafts of spiny neurons. The SPARn staining was eliminated by excess of the immunogen N-terminal peptide, but not by the C-terminal peptide (data not shown).

Taken together, the above results indicate that SPAR is specifically concentrated in excitatory synapses/spines of pyramidal neurons in hippocampal culture. However, a significant fraction of PSD-95 puncta did not costain for SPAR (Figure 5B1, arrows). SPAR was present in only 68.9% $\pm$ 4.0% of excitatory synapses on spiny neurons, based on colocalization with PSD-95 clusters. As comparison, GKAP was present at 90.6% $\pm$ 1.0% of PSD-95-positive synapses. We measured the integrated staining intensity of PSD-95 clusters, and divided them into two groups with intensity above, or

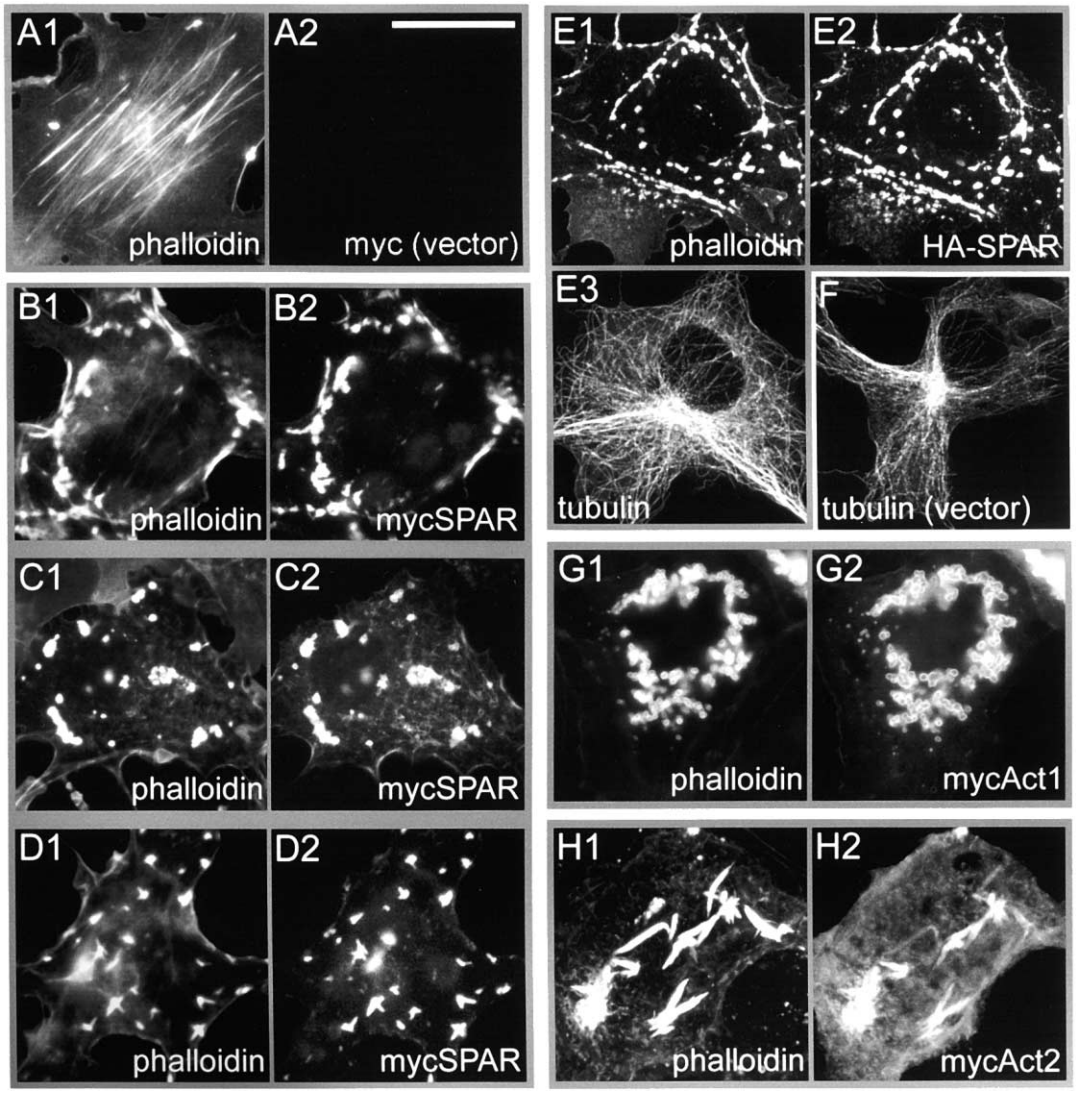

Figure 3. SPAR Reorganizes F-Actin in Heterologous Cells

(A) COS-7 cell transfected with vector only and stained with phalloidin-rhodamine to visualize F-actin (A1) and with myc antibody to determine the background level of myc staining (A2).

(B–D) COS cell transfected with myc-tagged SPAR and double-stained for F-actin (B1, C1, D1) and myc (B2, C2, D2).

(E) COS cell transfected with HA-tagged SPAR and triple-labeled for F-actin (E1), HA (E2), and α-tubulin (E3).

(F) Tubulin staining of a COS cell transfected with vector alone.

(G) COS cell transfected with myc-tagged SPAR Act1 domain and double-stained for F-actin (G1) and myc (G2).

(H) COS cell transfected with myc-tagged SPAR Act2 domain and double-stained for F-actin (H1) and myc (H2). Scale bar, 20 μm.

below, the mean. Only 8.8% ± 2.9% of the PSD-95 clusters with above-average staining intensity lacked associated SPAR staining, whereas 44.8% ± 4.5% of PSD-95 clusters with below-average intensity lacked SPAR (Figure 5C, inset).

In keeping with the finding that SPAR is not present at all PSD-95-positive synapses, SPAR immunoreactivity was detected in only 65.6% ± 1.1% of dendritic spines (which were "filled" by cotransfected GFP) (Figure 5C). The presence of SPAR correlated with larger spines; only 7.7% ± 1.1% of spines with head width larger than the mean (>0.67 μm) did not stain for SPAR, whereas 45.4% ± 1.3% of spines below the mean size lacked SPAR (Figure 5C, inset). Thus, the presence of SPAR correlates with large spine head size as well as abundance of PSD-95.

Spine Enlargement by SPAR

After transfection in cultured hippocampal neurons, HA epitope-tagged SPAR accumulated in the heads of dendritic spines (Figure 5D1, arrowheads), the latter being outlined by GFP expressed from a cotransfected plasmid (Figure 5D2). The punctate staining of HA-SPAR showed close apposition to synaptophysin (Figure 5F), and more precise colocalization with PSD-95 (Figure 5E), confirming the concentration of exogenous SPAR at postsynaptic sites.

We observed that a subset of dendritic spines on

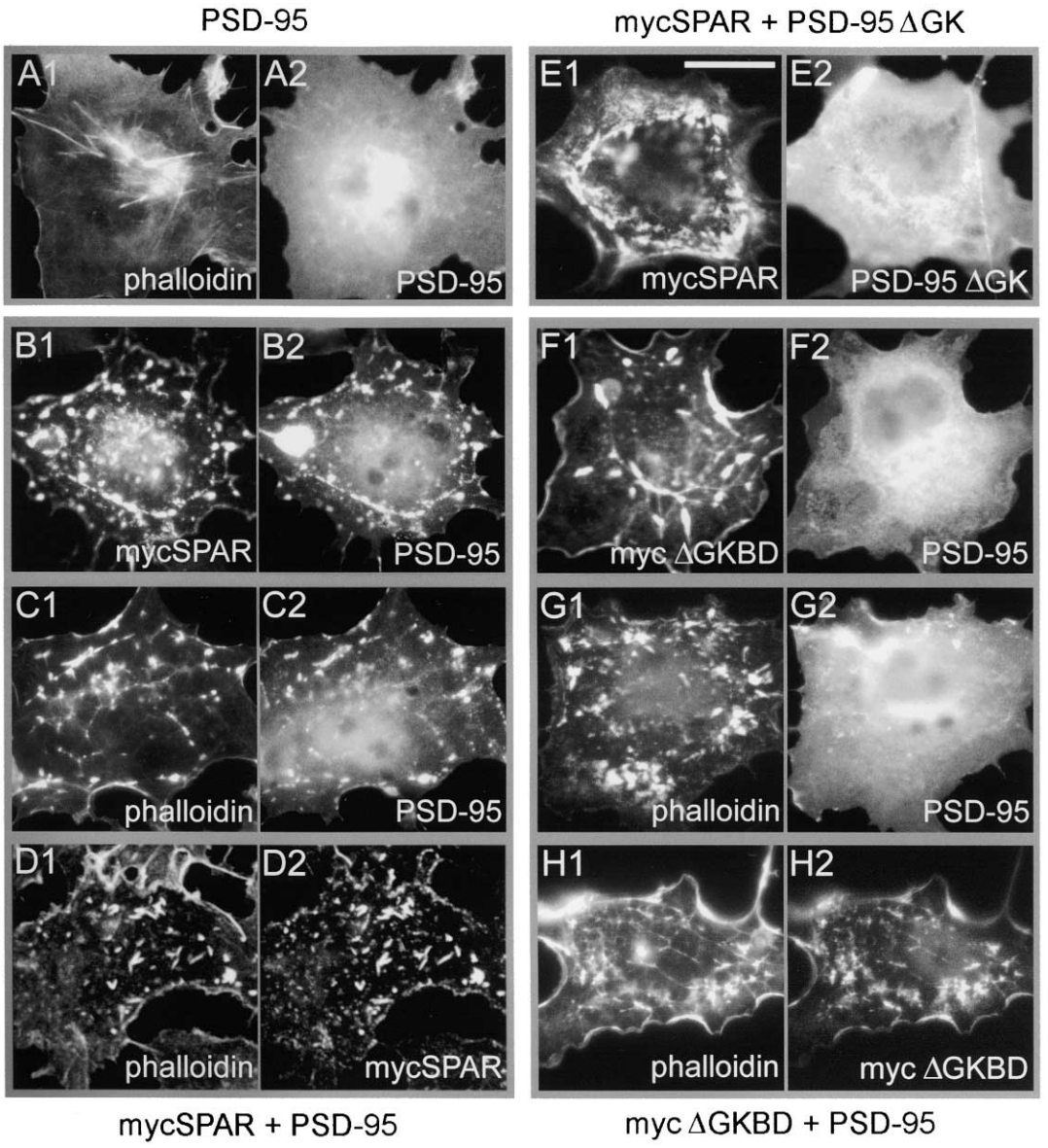

Figure 4. SPAR Recruits PSD-95 to F-Actin

(A) COS cell transfected with PSD-95 alone and double-stained for F-actin (A1) and for PSD-95 (A2).

(B–D) COS cells cotransfected with full-length PSD-95 and mycSPAR and double-stained for mycSPAR (B1, D2), PSD-95 (B2, C2), or F-actin (C1, D1).

(E) COS cell cotransfected with mycSPAR and PSD-95ΔGK and double-labeled for mycSPAR (E1) and PSD-95ΔGK (E2).

(F–H) COS cells cotransfected with PSD-95 and mycSPAR(ΔGKBD) and double-labeled for PSD-95 (F2, G2), SPAR ΔGKBD (F1, H2), or F-actin (G1, H1). Scale bar, 20 μm.

neurons expressing GFP + HA-SPAR ("SPAR neurons"; Figures 6B1 and 6C1, arrowheads) were larger than spines on control neurons transfected with GFP alone ("GFP neurons"; Figure 6A1). Using GFP expressed from a separate cotransfected plasmid to outline dendrites and spines, we measured the length of spines from the base of the neck to the furthest point on the spine head, and the maximal width of the spine head perpendicular to the long axis of the spine neck (see Figures 7D and 7H). The mean width of spine heads increased in SPAR neurons (0.86 ± 0.09 μm for SPAR neurons, versus 0.67 ± 0.09 μm for GFP neurons, $p < 0.001$). The maximum observed spine head width increased ~50%, from 1.5 μm in GFP control neurons to 2.3 μm in SPAR neurons. Due to limitations of the "GFP fill" approach and confocal microscopy, our measurements are not necessarily accurate in an absolute quantitative sense, but are valid for comparing relative dimensions between groups of neurons.

A frequency distribution plot of spine head widths revealed that a substantial proportion of spines in SPAR neurons were similar to control (peak between 0.4 and 0.6 μm) (Figure 7J); however, SPAR overexpression induced an additional major peak at 0.8–1.0 μm (Figure

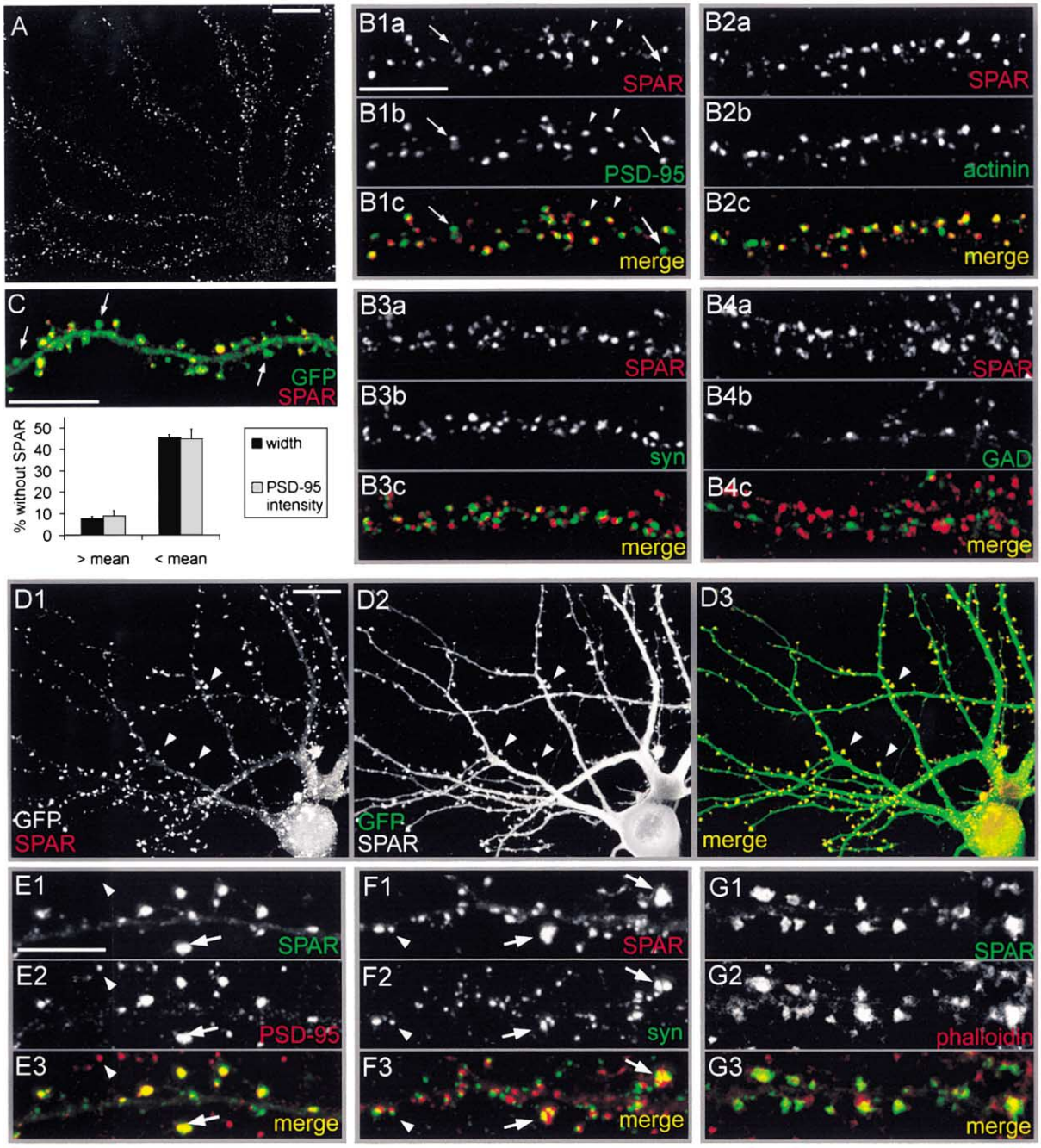

Figure 5. Postsynaptic Targeting of SPAR in Cultured Hippocampal Neurons

(A) Punctate dendritic staining of endogenous SPAR in a spiny neuron, using SPARn antibodies.

(B) Double labeling of hippocampal cultured neurons for endogenous SPAR (B1a, B2a, B3a, B4a) and PSD-95 (B1b), α-actinin (B2b), synaptophysin (B3b), and GAD (B4b), with merged color images in (B1c), (B2c), (B3c), and (B4c). SPAR colocalizes with a subset of PSD-95 clusters (arrowheads). Arrows, examples of PSD-95 clusters that lack SPAR.

(C) Dendrite of neuron transfected with GFP (green) and immunostained for endogenous SPAR (red). Arrows, examples of spines that lack SPAR. Inset, quantitation of spines and PSD-95 clusters that lack SPAR, grouped by spine head diameters or PSD-95 cluster intensity values above or below the mean.

(D) Neuron cotransfected with GFP and HA epitope-tagged SPAR and double-labeled for HA (D1, red) and GFP (D2, green), merge in (D3). HA-SPAR is enriched in dendritic spines (arrowheads).

(E–G) Dendrites from neurons transfected with HA-SPAR only, and double-labeled for HA-SPAR (E1, F1, G1) and for endogenous synaptic or spine markers: PSD-95 (E2), synaptophysin (F2), or F-actin (G2). Merged images in (E3), (F3), (G3). Arrowhead in (E) indicates a PSD-95 cluster from an untransfected neuron. Arrow in (E) indicates an enlarged spine from a SPAR-transfected neuron with increased PSD-95 immunoreactivity. Arrowhead in (F) indicates a spine from a SPAR-transfected neuron apposed to a single synaptophysin punctum. Arrows in (F) indicate enlarged spines from the same neuron contacting multiple distinct synaptophysin clusters. Scale bars = 5 μm for (A) and (D); 10 μm for (B) and (C) and (E–G).

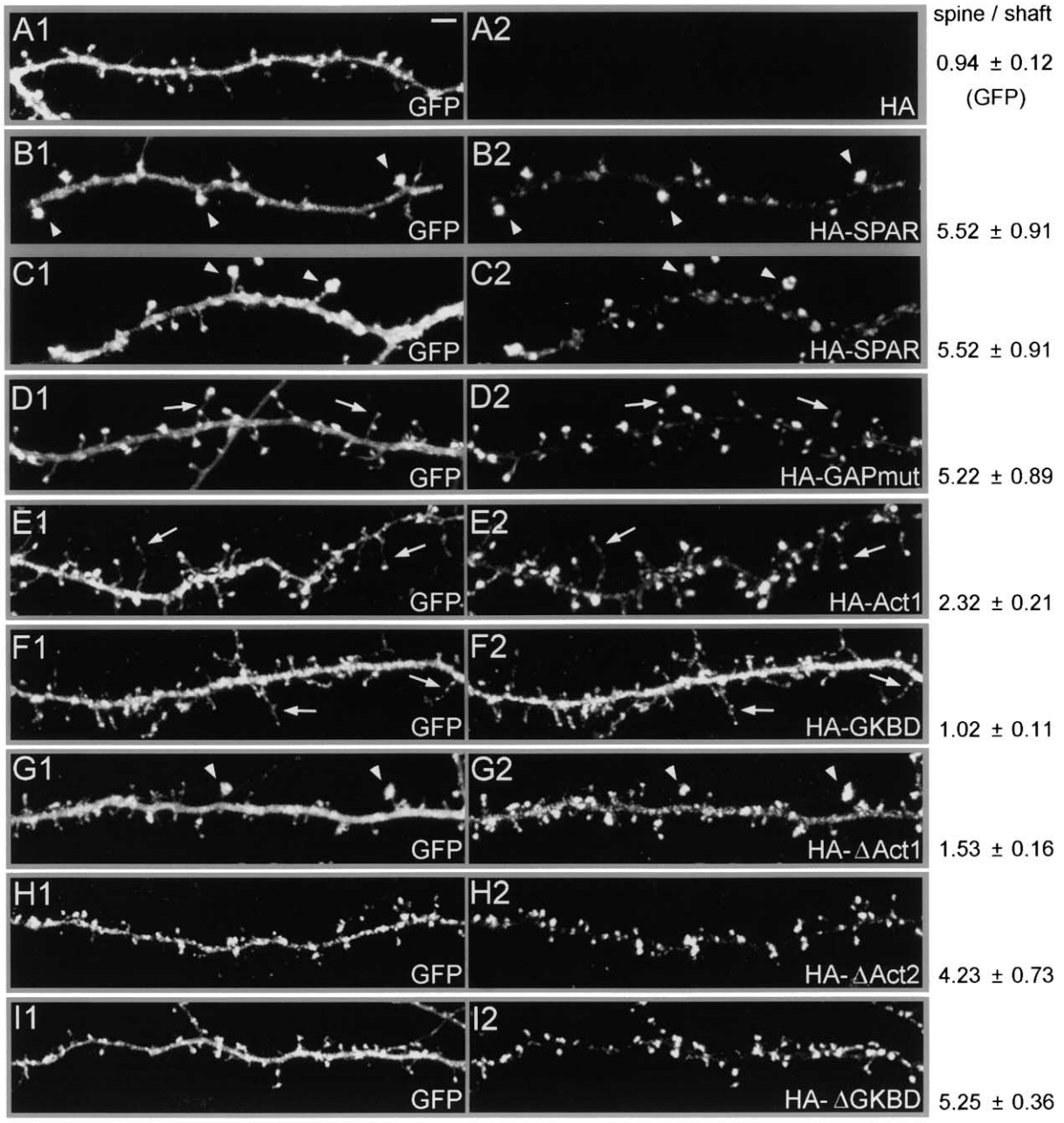

Figure 6. Spine Targeting of SPAR Mutants and Their Effects on Spine Morphology

(A–I) Dendrites from hippocampal neurons cotransfected with GFP and vector (A), HA tagged-SPAR (B and C), or SPAR mutants as indicated. Neurons were double-labeled for GFP to outline spine morphology (left panels) and for HA to localize the SPAR construct (right panels). Examples of enlarged spine heads are indicated by arrowheads (B, C, and G). Examples of elongated spines are indicated by arrows (D–F). Numbers on right indicate the ratio of fluoresence intensity in spines versus dendritic shafts of each construct (mean ± SEM), as index of spine targeting. Scale bar = 2 μm.

7J; see also cumulative distribution, Figure 7K). A comparison of representative spines at the 95th, 50th, 5th, and 1st percentiles (in order of increasing head size) illustrates the more pronounced difference between SPAR spines and control spines at the upper end of the distribution (Figures 7A–7H). SPAR had no significant effect on the mean length of spines (Figure 7L; 1.41 ± 0.12 μm for SPAR, versus 1.49 ± 0.23 μm for GFP, $p = 0.40$). Nevertheless, the spines with the largest heads in SPAR transfected neurons were often longer than average, but this effect could be attributed to the increase in head diameter.

The enlarged spine heads in SPAR neurons appeared to be postsynaptic compartments in the sense that they contained PSD-95 (Figure 5E) and were apposed to the presynaptic marker synaptophysin (Figure 5F). Indeed, the SPAR-enlarged spines showed more intense staining for PSD-95 (Figure 5E2, arrow) compared to spines

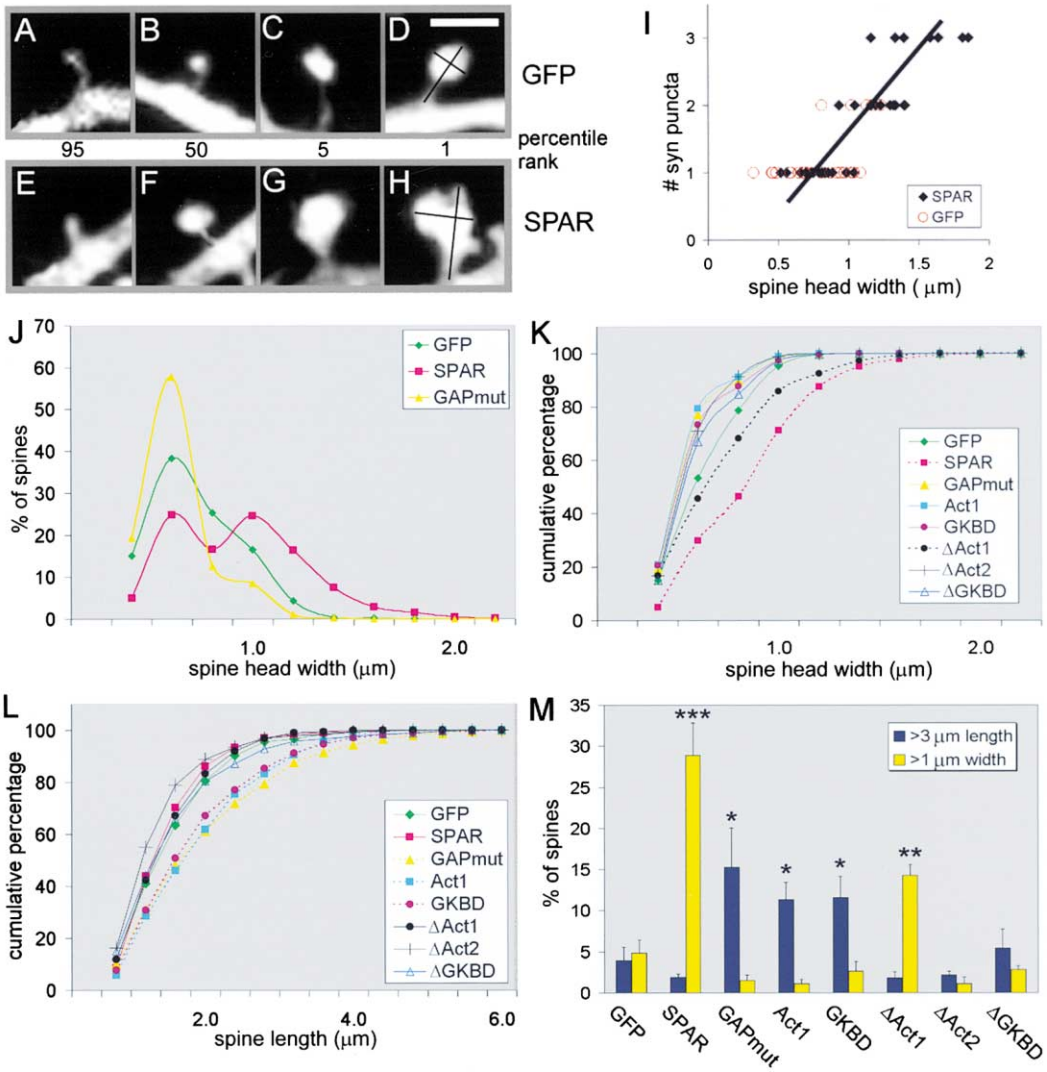

Figure 7. Morphometric Analysis of Spines in Neurons Transfected with SPAR and SPAR Mutants

(A–H) Spines from neurons transfected with GFP (A–D) or with SPAR + GFP (E–H) representing spines at the 95th (A and E), 50th (B and F), 5th (C and G), and highest (1st) percentile (D and H) of increasing spine head widths. The method used to measure spine dimensions is illustrated in (D) and (H). Scale bar, 2 μm.

(I) Number of distinct synaptophysin puncta apposed to spine heads as a function of spine head width in SPAR-transfected and control neurons.

(J) Frequency distribution of spine head widths in neurons transfected with indicated SPAR constructs or GFP-only control.

(K) Cumulative distribution of spine head widths in neurons transfected with SPAR constructs. Each distribution is significantly different from that of control GFP neurons (Kolmogorov-Smirnov test, $p < 0.0001$, except for ΔAct1 and ΔGKBD, $p < 0.005$).

(L) Cumulative distribution of spine lengths. Significantly longer spines than GFP control are observed for GAPmut, Act1, and GKBD, and significantly shorter spines for ΔAct2 ($p < 0.0001$, Kolmogorov-Smirnov test).

(M) Percentage of spines >3 μm length or >1 μm width in neurons transfected with indicated SPAR constructs (mean ± SEM). *$p < 0.01$, **$p < 0.001$, ***$p < 0.0001$ compared with GFP control (Student's t test).

of untransfected cells (Figure 5E2, arrowhead). Moreover, not only did the enlarged spines contact synaptophysin clusters (Figure 5F), the majority (64%) of spines of >1 μm width were apposed to more than one synaptophysin cluster (Figure 5F3, arrows, and data not shown). We found an approximately linear correlation between spine width and number of associated synaptophysin puncta in SPAR-transfected neurons (Figure 7I). In control GFP neurons, less than 2% of spines were apposed to more than a single synaptophysin punctum; these spines were at the upper end of the size distribution for GFP neurons (Figure 7I). These observations suggest that, along with spine head enlargement, SPAR promotes the growth of postsynaptic specializations and possibly the formation of multiple synapses on individual dendritic spines. However, these points require ultrastructural verification.

In transfected neurons, SPAR colocalized with F-actin, being highly enriched in dendritic spines (Figure 5G). In addition to spines, F-actin was often coaggregated with

exogenous SPAR within the cell bodies of neurons (data not shown), similar to the clusters induced by SPAR in COS cells. There were no dramatic changes in F-actin staining within dendritic shafts, which show low levels of phalloidin staining (Figure 5G2). No change was noted in the dendritic complexity of SPAR-transfected neurons (data not shown).

To determine which domains of SPAR were responsible for its targeting to spines, we transfected hippocampal neurons with various SPAR mutants. The targeting of each construct was quantified by the ratio of fluorescence intensity in spines versus dendritic shaft (Figure 6). For GFP, the mean spine/shaft ratio was 0.94 (Figure 6A1). Wild-type SPAR was highly enriched in spines (Figures 6B2 and 6C2), with a spine/shaft ratio of 5.52. Removal of the Act1 domain (ΔAct1) greatly impaired the concentration of SPAR in spines (Figure 6G2, spine/shaft ratio 1.53), indicating that Act1 is important for spine targeting. Consistent with this idea, the isolated Act1 domain was able to accumulate in spines (Figure 6E2, spine/shaft ratio 2.32). Mutation of the RapGAP domain, or deletion of Act2 or GKBD, had little effect on SPAR targeting (Figures 6D2, 6H2, and 6I2). In accordance, the isolated GKBD or Act2 domain were diffusely distributed in neurons (Figure 6F2, and data not shown). All the above SPAR constructs expressed at comparable levels (within 2-fold of HA-SPAR; data not shown), arguing that the differences in subcellular localization are not due to differences in expression level. We conclude that Act1 is a critical determinant for spine localization of SPAR.

Next, we assayed these same mutants for effects on spine enlargement in hippocampal neurons, cotransfecting GFP to outline spines. SPAR-GAPmut failed to induce expansion of spine heads; instead, spines became elongated (Figure 6D1, arrows; length = 1.78 ± 0.44 μm for GAPmut, versus 1.49 ± 0.23 μm for control, $p < 0.05$). This difference was also obvious from the cumulative distribution plot of spine lengths (Figure 7L). In addition, GAPmut caused a reduction in spine head width (Figures 7J and 7K; 0.44 ± 0.04 μm versus 0.67 ± 0.09 μm for GFP alone, $p < 0.01$). Thus, overexpression of GAPmut (which is unable to inactivate Rap) led to formation of longer and thinner spines, some of which resembled filopodia. These results suggest that Rap-GTP might promote spine elongation.

The SPAR mutant lacking Act1 (ΔAct1) still showed significant spine-enlarging activity (Figure 6G1), albeit less than wild-type SPAR (Figure 7K). Of the constructs tested, only wild-type SPAR (~6-fold) and ΔAct1 (~3-fold) increased the fraction of spines of >1 μm width (Figure 7M). Thus, the Act1 domain is not absolutely required for SPAR's ability to enlarge spines. That ΔAct1 is less effective in spine enlargement than wild-type SPAR could be explained by its relatively weak enrichment in spines (spine/shaft ratio of SPARΔAct1 = 1.53; Figure 6G2).

Unlike Act1, Act2 is not required for spine targeting of SPAR (Figure 6H2, spine/shaft ratio of ΔAct2 = 4.23), but its deletion abolished spine enlargement by SPAR (Figures 6H1 and 7K). In fact, ΔAct2 caused a shrinkage of spine heads (Figure 7K; 0.55 μm ± 0.03 versus 0.67 ± 0.09 μm for GFP control, $p < 0.01$), as well as a shortening of spine length, presumably due to its intact GAP domain (Figure 7L; 1.27 ± 0.11 μm versus 1.49 ± 0.23 μm for GFP, $p < 0.05$). The isolated Act2 domain overexpressed by itself had no effect on spines (data not shown), presumably because it cannot target to spines or synapses. Thus, Act2 appears to be critical for SPAR's ability to promote spine head growth; this may be related to the propensity of Act2 to reorganize F-actin in COS cells (see Figure 3H).

Deletion of the GKBD domain had no effect on spine localization of SPAR (ΔGKBD; Figure 6I2), presumably due to the intact targeting function of Act1. Despite its efficient spine targeting (spine/shaft ratio = 5.25), the ΔGKBD mutant of SPAR failed to induce spine enlargement (actually causing a significant reduction in spine head width), even though the Act2 domain was present (0.57 ± 0.05 μm versus 0.67 ± 0.09 μm for GFP, $p < 0.05$) (Figures 6I1, 7K, and 7M). These results suggest that interaction of SPAR with PSD-95 is essential for linking SPAR to its molecular targets involved in spine morphogenesis. In summary, three domains are crucial primarily for SPAR's spine enlarging activity: Act2, RapGAP, and GKBD. The fourth domain examined, Act1, appears primarily involved in spine targeting of SPAR.

Based on the above findings, we reasoned that interfering with Act1 or GKBD interactions should have dominant negative effects on endogenous SPAR function. Indeed, overexpression of either Act1 or GKBD as isolated domains (which should respectively interfere with spine targeting, or PSD-95 binding, of endogenous SPAR) led to the same effect: an increase in the length, and a decrease in the diameter, of a subset of spine heads (Figures 6E1 and 6F1; quantified in Figures 7K and 7L). Importantly, this effect was essentially identical to the dominant negative phenotype induced by the GAPmut (Figures 6D1, 7K, and 7L). Counting the percentage of spines >3 μm in length highlights the spine elongation phenotype induced by GAPmut, Act1, and GKBD (Figure 7M). Taken together, these data uncovered two functions of endogenous SPAR: to suppress the elongation of spines via GAP activity and to promote spine head enlargement via Act2.

Alteration of Dendritic Spine Shape by SPAR

Concomitant with an increase in the size of spine heads, we observed a striking effect of SPAR on the shape of dendritic spines. Spine shape is developmentally regulated, generally progressing from filopodia in early development to "stubby," "thin," or "mushroom" shaped spines in mature brain or cultured neurons (Ziv and Smith, 1996; Fiala et al., 1998; Harris, 1999). In the hippocampal neurons used here (~17–21 DIV), ~60% of the dendritic spines on pyramidal cells are mushroom-shaped (Figure 8M), with a thin neck and a single well-defined head that is relatively smooth in contour and globular in shape (e.g., Figure 8A). In SPAR-transfected neurons, however, a substantial proportion of spines, particularly larger spines, were highly irregular in shape (compare Figure 8A with Figure 8F; quantified in Figure 8N). The irregularity of spine shape in SPAR neurons was of two major types: "thorny" spines with sharp projections or outgrowths (Figures 8G–8I), and "multilobed" spines which appeared to have multiple "heads" fused together atop a single neck (Figures 8J–8L). We also

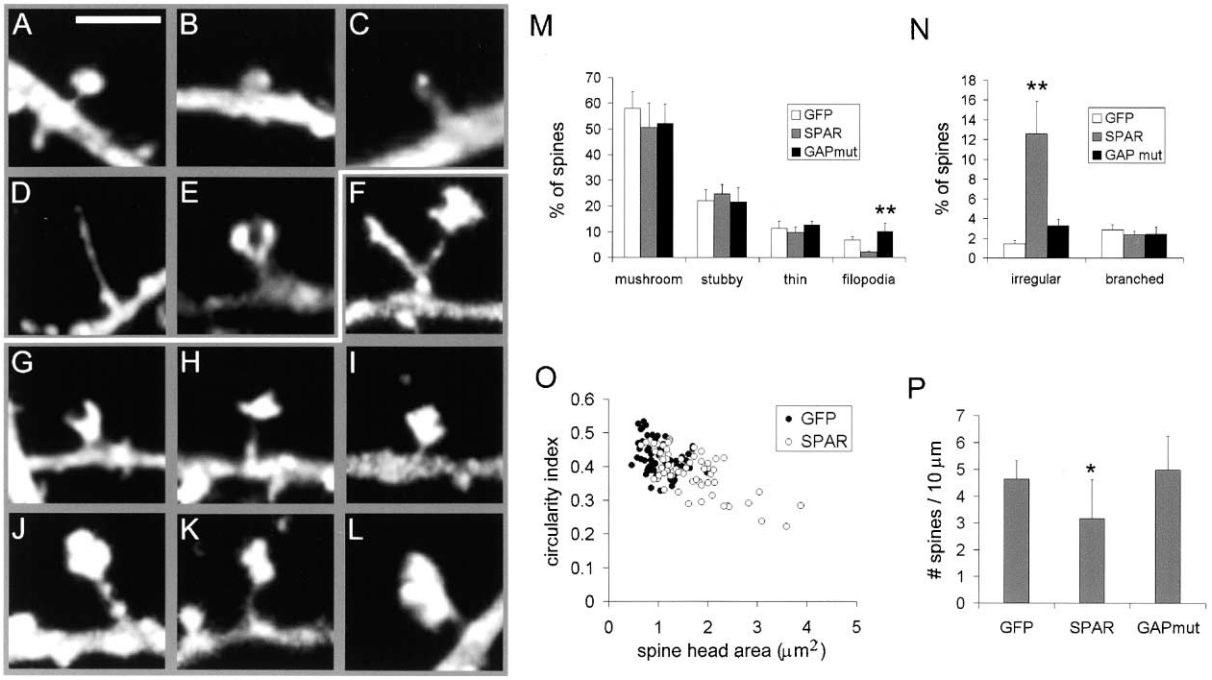

Figure 8. Effect of SPAR on Dendritic Spine Shape

(A–L) Representative images of spines in different morphological categories. In each case the image was acquired by visualizing cotransfected GFP.

(A–E) Examples of morphologies of dendritic spines on control neurons transfected with GFP alone. (A) Mushroom spine. (B) Stubby spine. (C) Thin spine. (D) Filopodium. (E) Branched spine.

(F–L) Examples of irregular spines from neurons cotransfected with SPAR + GFP. (F) Branched and thorny spine.

(G–I) Examples of unbranched thorny spines.

(J–L) Examples of multilobed spines.

(M) Percentage of spines in the different morphological categories (mean ± SEM) from GFP, SPAR + GFP ("SPAR"), or GAPmut + GFP ("GAPmut") transfected neurons. **$p < 0.005$, SPAR versus GAPmut (Student's t test).

(N) Percentage of irregular spines (thorny or multilobed) and of branched spines in GFP-, SPAR-, or GAPmut-transfected neurons (mean ± SEM). ** $p < 0.005$, GFP versus SPAR, Student's t test.

(O) Circularity index of spines from GFP- or SPAR-transfected neurons plotted against spine head area.

(P) Quantitation of the spine density (number of spines/10 μm dendrite length) in the same neuronal populations as above (mean ± SEM). *$p < 0.05$, GFP versus SPAR, Student's t test. Scale bar = 4 μm.

measured the maximal crosssectional area of spines by tracing the outlines of the heads using z-series stacks of confocal images, which confirmed that the SPAR neurons possessed larger spines than GFP neurons in terms of spine head area (Figure 8O). The degree of irregularity of spine heads was quantified by the circularity index: the lower the index, the more complex the shape, with a maximal value of 1 for a perfect circle (see Experimental Procedures, and Amaral and Dent, 1981). Plotting area against the circularity index confirmed that spines from SPAR neurons were more complex than those from GFP neurons and established that irregularity was correlated with increased spine head area (Figure 8O). The percentage of branched spines (spines that have two heads and two necks that merge into a single neck at the base; e.g., Figures 8E and 8F) was similar in SPAR and GFP neurons (Figure 8N). Furthermore, SPAR neurons developed slightly fewer spines than control (Figure 8P), making it unlikely that SPAR promotes spine formation.

The relative distribution of spine shapes did not appear to be affected by SPAR, with similar percentages of mushroom, stubby, and thin spines in GFP and SPAR neurons (Figure 8M). However, filopodia (long spines lacking a discernible head) were virtually absent from SPAR neurons, whereas neurons transfected with GAPmut SPAR (R807A/T808S mutant) showed an increase in the number of filopodia (Figure 8M). In addition, irregularity of dendritic spine morphology was not seen in neurons transfected with GAPmut SPAR (Figure 8N). Thus, RapGAP activity is required for both the enlargement of spine heads and for the increased complexity of spine shape induced by SPAR, implicating Rap signaling in the regulation of spine morphology.

Discussion

SPAR-PSD-95 Interaction and Implications for Postsynaptic Rap Signaling

We have identified SPAR as a member of the "inner circle" of PSD-95-associated proteins, binding directly to the GK domain of PSD-95/SAP90 family members. This interaction includes SPAR in a large group of postsynaptic proteins that includes NMDA receptors and their downstream signaling targets (Husi et al., 2000; Sheng and Pak, 2000; Walikonis et al., 2000). SPAR brings to the NMDA receptor/PSD-95 complex the ability

to stimulate the GTPase activity of Rap, especially Rap2. Regulation by GAPs may be particularly important for Rap proteins because of their low intrinsic GTPase activity relative to other small GTPases. Rap1 is responsive to a wide range of extracellular stimuli and can be activated in various systems by Ca^{2+}, diacylglycerol, and cAMP (Zwartkruis and Bos, 1999). Such second messengers can be generated postsynaptically via multiple mechanisms, e.g., activation of NMDA receptors, metabotropic glutamate receptors, voltage-gated calcium channels, or dopamine receptors. Very little is known about the function of Rap2, which is 60% identical to Rap1. Of relevance is that Rap2, but not Rap1, was recently identified in the NMDA receptor complex by coimmunoprecipitation (Husi et al., 2000). By immunostaining, Rap2 is expressed in neurons and its distribution overlaps with that of PSD-95 (D.P., M.S., unpublished data). These observations, along with the apparent preference of SPAR for Rap2, makes Rap2 the probable Rap GTPase regulated by SPAR and NMDA receptors at postsynaptic sites.

SPAR Regulation of Actin Cytoskeleton

SPAR had a striking effect on the actin cytoskeleton in heterologous cells, mediated by two independent domains, Act1 and Act2. Act1 and Act2 probably interact with the actin cytoskeleton via distinct mechanisms, because these domains lack sequence similarity, have different effects on F-actin organization in COS cells, and are differentially involved in spine targeting and spine enlargement in neurons. Whether direct or indirect, physical association of SPAR and F-actin is suggested by the tight colocalization of SPAR and phalloidin staining in all cells examined. Our results also indicate that SPAR can recruit PSD-95 to the actin cytoskeleton in a manner dependent on the GKBD of SPAR and the GK domain of PSD-95. The simplest explanation is that SPAR can act as a bridging molecule between the PSD-95 complex and F-actin, the predominant cytoskeleton in dendritic spines.

Precedent for Rap and RapGAP involvement in localized actin remodeling is found in the budding yeast *S. cerevisiae*, in which the Rap homolog Bud1 and its GAP (Bud2) target polarity factors involved in cytoskeletal organization to the site of bud formation. Among these factors are Cdc42 and its GEF, Cdc24 (Chant, 1999). By analogy to yeast bud formation, SPAR and Rap2 could function in dendritic spines as a targeting mechanism or organizer for regulators of actin polymerization such as Cdc42, particularly in light of recent work showing direct binding of Rap2 to actin (Torti et al., 1999) and spine altering effects of Rho family GTPases in neurons (Nakayama et al., 2000; Penzes et al., 2001).

Role of SPAR in Dendritic Spines

In cultured hippocampal neurons, SPAR is enriched particularly in large spines, suggesting a role in spine growth and maturation. Consistent with this proposed function, SPAR exerts a local effect on the morphology of spine heads, causing an enlargement and an increase in complexity of spine shape when overexpressed. These morphological effects require three domains of SPAR: GKBD, RapGAP, and Act2. Because GKBD has no recognizable catalytic activity and does not alter the actin cytoskeleton in COS cells (data not shown), it presumably functions primarily as a protein interaction site that is important for localizing SPAR in molecular proximity of its targets (such as Rap2 or a regulator of actin polymerization). The simplest model is that SPAR function in spines depends on its interaction with the PSD-95 signaling complex, as mediated by the binding of GKBD to PSD-95.

The requirement for SPAR GAP activity in spine enlargement implicates endogenous Rap signaling in spine morphogenesis. Based on the phenotype of GAPmut overexpression (which should disinhibit Rap in spines), we propose that Rap-GTP activates a pathway that leads to emaciation and elongation of spines. The function of SPAR is at least in part to counteract this activity of Rap, leading to cessation of longtitudinal spine growth. Consistent with this model, the dominant negative constructs Act1 and GKBD shared with GAPmut the phenotype of longer, narrower spines. An additional activity of SPAR is to stimulate the latitudinal growth of the spine (spine head enlargement) with accompanying increase in morphological complexity of the spine head. This activity requires domain Act2, which has powerful effects on F-actin organization. Because the GAPmut (which retains Act2) is ineffective at spine head enlargement, we infer that Rap activity on elongation is "dominant," i.e., Rap needs to be inhibited before SPAR can induce equatorial expansion of the spine head. Overall, our data point to an antagonistic relationship between Rap and SPAR in regulation of spine structure, with activated Rap favoring spines with more immature filopodia-like morphology.

SPAR also caused a small but significant decrease in spine density, an effect dependent on a functional GAP domain. One reasonable explanation for this effect is that SPAR overexpression inhibits endogenous Rap activity in developing spines, leading to inhibition of filopodial extension. Because filopodia are thought to be precursors of mature spines, and filopodia/spine turnover occurs continuously even in mature cultures (Boyer et al., 1998), an inhibition by SPAR of filopodial extension would be expected to lead to reduced spine numbers over the course of the experiment (3–4 days of SPAR overexpression). This possibility is supported by the virtual absence of filopodia in neurons overexpressing SPAR (Figure 8M).

What is the functional significance of SPAR-induced changes in dendritic spine structure? Synapses are typically formed on the heads of spines, and there is a positive correlation between the size of spines and the size of synapses associated with those spines (Harris and Kater, 1994). The enlarged spine heads induced by SPAR contain higher levels of PSD-95 immunoreactivity, consistent with an expansion of the PSD. Indeed, SPAR-enlarged spines were frequently associated with multiple discrete puncta of synaptophysin staining, suggesting that these spines may have developed multiple synaptic contacts. Ultrastructural analysis will be required, however, to establish this definitively.

The highly irregular appearance of many spines in SPAR-overexpressing neurons is suggestive of spines that are dividing. It is controversial whether spine division is a structural correlate of synaptic plasticity (Nieto-

Sampedro et al., 1982; Carlin and Siekevitz, 1983; Sorra et al., 1998). However, a recent EM study, which identified potentiated synapses, provided evidence that structural spine changes (perforation and multispine synapse formation) indeed accompany LTP (Toni et al., 1999). Based on the effects of SPAR on spine morphology, we speculate that postsynaptic Rap and SPAR might regulate actin polymerization during growth and splitting of dendritic spines.

Other proteins have been shown to alter spine morphology. For example, drebrin is an actin binding protein that causes spine elongation, without apparent effect on spine head size (Hayashi and Shirao, 1999). Shank is a scaffolding protein of the PSD that induces enlargement but not irregularity of spine heads (Sala et al., 2001). Rac1 promotes loss of dendritic spines, accompanied by the formation of filopodia and ruffles (Nakayama et al., 2000), while overexpression of Kalirin-7, a GEF for Rac1, causes a similar formation of aberrant spine-like structures including lamellipodia, ruffles, and filopodia (Penzes et al., 2001). The effects of SPAR on spines differ from the above proteins; for instance, SPAR affects only a subset of spines, and it increases both the size and complexity of the spine head without inducing lamellipodia and ruffles. Clearly, multiple distinct molecular mechanisms impinge on spine morphology, and it will be important to determine how such mechanisms are integrated to control the structure of these specialized postsynaptic compartments.

Experimental Procedures

Yeast Two-Hybrid

Two-hybrid screen and assays were performed using the yeast strain L40 harboring β-gal and HIS3 reporters, as described (Niethammer and Sheng, 1999). 1×10^6 clones of a rat brain cDNA library in pGAD10 (Clontech) were screened using as bait the combined SH3-GK domains of chapsyn-110 (aa 522–852) cloned in pBHA.

DNA Constructs

Complete SPAR cDNA was obtained by PCR from a rat brain Marathon library using specific primers (GenBank accession #AF026504). The product was cloned into the mammalian expression vector pGW1 with the addition of N-terminal myc or HA epitope tag. Deletion constructs were generated by PCR with appropriate primers, and cloned into pGW1 or pGAD10. Site directed mutagenesis was performed using "QuikChange" (Stratagene). All constructs were verified by DNA sequencing. H-Ras, Rap1A, and Rap2A clones in pGEX were gifts of Jean de Gunzburg (Janoueix-Lerosey et al., 1998). The following constructs have been described: Kv1.4 C terminus in pBHA, and PSD-95 PDZ1/2 in pGAD10 (Kim et al., 1995), PSD-95 family GK domains in pBHA, and PSD-95 and PSD-95ΔGK in GW1 (Kim et al., 1997), and Tbr1 in pGAD10 (Hsueh et al., 2000).

Antibodies

SPAR antibodies were generated by immunizing rabbits with peptides corresponding to aa 1744–1760 (SPARc) and aa 4–20 (SPARn) of SPAR, and affinity purified on a column of covalently coupled peptide. The following antibodies have been described: guinea pig PSD-95 (Kim et al., 1995), SynGAP (Kim et al., 1998), GluR1 (Blackstone et al., 1992), NR2B (Sheng et al., 1994). K28/43 (PSD-95 specific) and K28/86 (pan-PSD-95) monoclonal antibodies were gifts from J. Trimmer (SUNY Stony Brook). The following antibodies were purchased from commercial sources: myc 9E10, myc agarose conjugate, HA rabbit polyclonal (Santa Cruz Biotechnology); GFP monoclonal 3E6 (Quantum Biotechnologies); GAD (Boehringer Mannheim); α-tubulin B-5-1-2, α-actinin A7811, and synaptophysin SVP38 monoclonals (Sigma).

COS-7 Transfections, Immunostaining, and Immunoprecipitation

COS-7 cells were transfected using Lipofectamine (Gibco BRL) and immunostained as described (Kim et al., 1995). For immunoprecipitation, cells were harvested in RIPA buffer, and lysates centrifuged at 100,000 × g for 15 min. Myc antibody (9E10)-coupled agarose, PSD-95 antibody K28/43, or nonimmune rabbit and mouse IgG/protein A sepharose conjugates were mixed with supernatants for 2 hr at 4°C. After washing 5× in RIPA buffer, immunoprecipitates were analyzed by immunoblotting.

Immunoprecipitation and Fractionation of Brain Lysates

Immunoprecipitations from rat brain homogenates were performed as described (Dunah et al., 1998), except that whole brain lysates were extracted by 1% sodium deoxycholate for 1 hr at 4°C. For each immunoprecipitation, clarified extract (200 μg protein) was incubated with 10 μg of SPARc antibodies (or rabbit IgG) for 2 hr at 4°C. For peptide competition experiments, 50 μg (~100 μM) of peptide was added to the extract prior to addition of antibodies. Precipitates were washed in 50 mM Tris (pH 7.5), 150 mM NaCl, and 0.1% Triton X-100. PSD purification (Cho et al., 1992), and subcellular biochemical fractionation (Huttner et al., 1983) of rat brain were performed as described.

In Vitro GAP Assay

COS-7 cells transfected with myc-tagged SPAR were lysed with GAP lysis buffer (20 mM Tris [pH 7.4], 100 mM NaCl, 5 mM $MgCl_2$, 1% NP40, 0.5% deoxycholate, 1 mM DTT) 24 hr posttransfection, and immunoprecipitated with 9E10-agarose beads. Precipitates were washed 4× in lysis buffer and 2× in GAP assay buffer (20 mM Tris [pH 7.4], 100 mM NaCl, 10 mM $MgCl_2$, 1 mM DTT, and 40 μg/ml BSA). GST-H-Ras, -Rap1A, and -Rap2A were expressed in BL21 *E. coli* and purified on glutathione sepharose. Purified GTPases (0.25 μM final concentration) were incubated for 15 min at 30°C in loading buffer (50 mM Tris [pH 7.4], 2 mM EDTA, 100 mM NaCl, 0.1 mM DTT, 0.5 mg/ml BSA, and 0.005% DOC) containing 0.2 μM [^{32}P]γ-GTP. GTP-loaded GTPases were diluted 20-fold in ice-cold GAP assay buffer that included 20 μM unlabeled GTP and then apportioned to immunoprecipitates from COS-7 cell lysates. GAP reactions were performed at 30°C with continuous mixing to maintain mycSPAR beads in suspension and quenched with ten volumes of ice-cold stop buffer (20 mM Tris [pH 7.4], 1 mM $MgCl_2$). After filtering through BA85 nitrocellulose (Schleicher and Schuell) to recover GTPases, the amount of bound radiolabel was quantified by liquid scintillation counting.

Neuronal Culture, Transfection, and Immunostaining

For spine morphology studies, hippocampal primary neuronal cultures prepared from embryonic day (E) 18–19 rat embryos were plated at high density (~750 cells mm^{-2}) (Sala et al., 2000). For colocalization studies, medium density cultures (~150 cells mm^{-2}) were plated on coverslips coated with poly-D-lysine (30 μg/ml) and laminin (2 μg/ml). Cultures were grown in Neurobasal medium (Gibco BRL) supplemented with B27 (Gibco BRL), 0.5 mM glutamine, and 12.5 μM glutamate. Neurons were transfected at ~14 DIV using calcium phosphate (Xia et al., 1996). Three to seven days posttransfection, immunostaining was performed as described (Sala et al., 2000).

Quantitation

Images were acquired using an MRC1024 confocal microscope (Bio-Rad). Confocal z-series image stacks encompassing entire dendrite segments were analyzed using MetaMorph software (Universal Imaging Corporation). For quantitation of spine size, measurements were obtained in the GFP channel using identical confocal settings for each sample and counting at least 1000 spines per construct (from six to ten neurons). For all other quantitations, three to four dendritic segments of 100 μm were collected from at least six neurons. For each construct, individual spine measurements were first grouped and averaged per neuron; means from several neurons were then averaged to obtain a population mean (presented as mean ± SEM). Statistical significance between two means was calculated using Student's t test. To quantify irregularity of spine shape, outlines of spine heads were traced from confocal z-series stacks,

and the index of circularity R calculated with the formula $R = 4\pi$ area / perimeter^2 (Amaral and Dent, 1981).

Acknowledgments

We thank J. de Gunzburg for GST fusion constructs of small GTPases and R. Huganir for SynGAP antibodies. M.S. is Assistant Investigator of the Howard Hughes Medical Institute. This work was supported by the Brain Science Research Program of the Korean Ministry of Science and Technology (E.K.) and NIH grants NS10886 (D.P.) and NS35050 (M.S.).

Received October 25, 2000; revised May 10, 2001.

References

Amaral, D.G., and Dent, J.A. (1981). Development of the mossy fibers of the dentate gyrus: I. A light and electron microscopic study of the mossy fibers and their expansions. J. Comp. Neurol. *195*, 51–86.

Bailey, C.H., and Kandel, E.R. (1993). Structural changes accompanying memory storage. Annu. Rev. Physiol. *55*, 397–426.

Blackstone, C.D., Moss, S.J., Martin, L.J., Levey, A.I., Price, D.L., and Huganir, R.L. (1992). Biochemical characterization and localization of a non-*N*-methyl-D-aspartate glutamate receptor in rat brain. J. Neurochem. *58*, 1118–1126.

Boettner, B., Govek, E.E., Cross, J., and Van Aelst, L. (2000). The junctional multidomain protein AF-6 is a binding partner of the Rap1A GTPase and associates with the actin cytoskeletal regulator profilin. Proc. Natl. Acad. Sci. USA *97*, 9064–9069.

Boyer, C., Schikorski, T., and Stevens, C.F. (1998). Comparison of hippocampal dendritic spines in culture and in brain. J. Neurosci. *18*, 5294–5300.

Cabib, E., Drgonova, J., and Drgon, T. (1998). Role of small G proteins in yeast cell polarization and wall biosynthesis. Annu. Rev. Biochem. *67*, 307–333.

Carlin, R.K., and Siekevitz, P. (1983). Plasticity in the central nervous system: do synapses divide? Proc. Natl. Acad. Sci. USA *80*, 3517–3521.

Caron, E., Self, A.J., and Hall, A. (2000). The GTPase Rap1 controls functional activation of macrophage integrin alphaMbeta2 by LPS and other inflammatory mediators. Curr. Biol. *10*, 974–978.

Chang, F.L., and Greenough, W.T. (1984). Transient and enduring morphological correlates of synaptic activity and efficacy change in the rat hippocampal slice. Brain Res. *309*, 35–46.

Chant, J. (1999). Cell polarity in yeast. Annu. Rev. Cell Dev. Biol. *15*, 365–391.

Chen, H.J., Rojas-Soto, M., Oguni, A., and Kennedy, M.B. (1998). A synaptic Ras-GTPase activating protein (p135 SynGAP) inhibited by CaM kinase II. Neuron *20*, 895–904.

Cho, K.-O., Hunt, C.A., and Kennedy, M.B. (1992). The rat brain postsynaptic density fraction contains a homolog of the Drosophila discs-large tumor suppressor protein. Neuron *9*, 929–942.

Crick, F. (1982). Do dendritic spines twitch? Trends Neurosci. *5*, 44–46.

Deguchi, M., Hata, Y., Takeuchi, M., Ide, N., Hirao, K., Yao, I., Irie, M., Toyoda, A., and Takai, Y. (1998). BEGAIN (brain-enriched guanylate kinase-associated protein), a novel neuronal PSD-95/SAP90-binding protein. J. Biol. Chem. *273*, 26269–26272.

Desmond, N.L., and Levy, W.B. (1988). Synaptic interface surface area increases with long-term potentiation in the hippocampal dentate gyrus. Brain Res. *453*, 308–314.

Dunah, A.W., Luo, J., Wang, Y.H., Yasuda, R.P., and Wolfe, B.B. (1998). Subunit composition of N-methyl-D-aspartate receptors in the central nervous system that contain the NR2D subunit. Mol. Pharmacol. *53*, 429–437.

Engert, F., and Bonhoeffer, T. (1999). Dendritic spine changes associated with hippocampal long-term synaptic plasticity. Nature *399*, 66–70.

Fiala, J.C., Feinberg, M., Popov, V., and Harris, K.M. (1998). Synaptogenesis via dendritic filopodia in developing hippocampal area CA1. J. Neurosci. *18*, 8900–8911.

Fifkova, E., and Van Harreveld, A. (1977). Long-lasting morphological changes in dendritic spines of dentate granular cells following stimulation of the entorhinal area. J. Neurocytol. *6*, 211–230.

Fischer, M., Kaech, S., Knutti, D., and Matus, A. (1998). Rapid actin-based plasticity in dendritic spines. Neuron *20*, 847–854.

Gao, Q., Srinivasan, S., Boyer, S.N., Wazer, D.E., and Band, V. (1999). The E6 Oncoproteins of High-Risk Papillomaviruses Bind to a Novel Putative GAP Protein, E6TP1, and Target It for Degradation. Mol. Cell. Biol. *19*, 733–744.

Halpain, S., Hipolito, A., and Saffer, L. (1998). Regulation of F-actin stability in dendritic spines by glutamate receptors and calcineurin. J. Neurosci. *18*, 9835–9844.

Harris, K.M. (1999). Structure, development, and plasticity of dendritic spines. Curr. Opin. Neurobiol. *9*, 343–348.

Harris, K.M., and Kater, S.B. (1994). Dendritic spines: cellular specializations imparting both stability and flexibility to synaptic function. Annu. Rev. Neurosci. *17*, 341–371.

Hattori, M., Tsukamoto, N., Nur-e-Kamal, M., Rubinfeld, B., Iwai, K., Kubota, H., Maruta, H., and Minato, N. (1995). Molecular cloning of a novel mitogen-inducible nuclear protein with a Ran GTPase-activating domain that affects cell cycle progression. Mol. Cell. Biol. *15*, 552–560.

Hayashi, K., and Shirao, T. (1999). Change in the shape of dendritic spines caused by overexpression of drebrin in cultured cortical neurons. J. Neurosci. *19*, 3918–3925.

Horner, C.H. (1993). Plasticity of the dendritic spine. Prog. Neurobiol. *41*, 281–321.

Hsueh, Y.P., Wang, T.F., Yang, F.C., and Sheng, M. (2000). Nuclear translocation and transcription regulation by the membrane-associated guanylate kinase CASK/LIN-2. Nature *404*, 298–302.

Husi, H., Ward, M., Choudhary, J., Blackstock, W., and Grant, S. (2000). Proteomic analysis of NMDA receptor-adhesion protein signaling complexes. Nat. Neurosci. *3*, 661–669.

Huttner, W., Schiebler, W., Greengard, P., and DeCamilli, P. (1983). Synapsin I (protein I), a nerve terminal-specific phosphoprotein. III. Its association with synaptic vesicles studied in a highly purified synaptic vesicle preparation. J. Cell Biol. *5*, 1374–1388.

Janoueix-Lerosey, I., Pasheva, E., De Tand, M.-F., Tavitian, A., and De Gunzburg, J. (1998). Identification of a specific effector of the small GTP-binding protein Rap *2*. Eur. J. Biochem. *252*, 290–298.

Kim, E., Cho, K.-O., Rothschild, A., and Sheng, M. (1996). Heteromultimerization and NMDA receptor-clustering activity of chapsyn-110, a member of the PSD-95 family of proteins. Neuron *17*, 103–113.

Kim, E., Naisbitt, S., Hsueh, Y.-P., Rao, A., Rothschild, A., Craig, A.M., and Sheng, M. (1997). GKAP, a novel synaptic protein that interacts with the guanylate kinase-like domain of the PSD-95/SAP90 family of channel clustering molecules. J. Cell Biol. *136*, 669–678.

Kim, E., Niethammer, M., Rothschild, A., Jan, Y.N., and Sheng, M. (1995). Clustering of shaker-type K^+ channels by interaction with a family of membrane-associated guanylate kinases. Nature *378*, 85–88.

Kim, J.H., Liao, D., Lau, L.F., and Huganir, R.L. (1998). SynGAP: a synaptic RasGAP that associates with the PSD-95/SAP90 protein family. Neuron *20*, 683–691.

Kistner, U., Wenzel, B.M., Veh, R.W., Cases-Langhoff, C., Garner, A.M., Appeltauer, U., Voss, B., Gundelfinger, E.D., and Garner, C.C. (1993). SAP90, a rat presynaptic protein related to the product of the *Drosophila* tumor suppressor gene *dlg*-A. J. Biol. Chem. *268*, 4580–4583.

Kornau, H.-C., Schenker, L.T., Kennedy, M.B., and Seeburg, P.H. (1995). Domain interaction between NMDA receptor subunits and the postsynaptic density protein PSD-95. Science *269*, 1737–1740.

Kurachi, H., Wada, Y., Tsukamoto, N., Maeda, M., Kubota, H., Hattori, M., Iwai, K., and Minato, N. (1997). Human SPA-1 gene product selectively expressed in lymphoid tissues is a specific GTPase-

activating protein for Rap1 and Rap2. Segregate expression profiles from a rap1GAP gene product. J. Biol. Chem. *272*, 28081–28088.

Maletic-Savatic, M., Malinow, R., and Svoboda, K. (1999). Rapid dendritic morphogenesis in CA1 hippocampal dendrites induced by synaptic activity. Science *283*, 1923–1927.

Matus, A. (2000). Actin-based plasticity in dendritic spines. Science *290*, 754–758.

McKinney, R.A., Capogna, M., Durr, R., Gahwiler, B.H., and Thompson, S.M. (1999). Miniature synaptic events maintain dendritic spines via AMPA receptor activation. Nat. Neurosci. *2*, 44–49.

Nakayama, A.Y., Harms, M.B., and Luo, L. (2000). Small GTPases Rac and Rho in the maintenance of dendritic spines and branches in hippocampal pyramidal neurons. J. Neurosci. *20*, 5329–5338.

Niethammer, M., Kim, E., and Sheng, M. (1996). Interaction between the C terminus of NMDA receptor subunits and multiple members of the PSD-95 family of membrane-associated guanylate kinases. J. Neurosci. *16*, 2157–2163.

Niethammer, M., and Sheng, M. (1999). Identification of ion channel-associated proteins using the yeast two-hybrid system. In Methods Enzymology., P.M. Conn, ed. (New York: Academic Press), pp. 104–122.

Nieto-Sampedro, M., Hoff, S.F., and Cotman, C.W. (1982). Perforated postsynaptic densities: probable intermediates in synapse turnover. Proc. Natl. Acad. Sci. USA *79*, 5718–5722.

Noda, M. (1993). Mechanisms of reversion. Faseb. J. *7*, 834–840.

Ohtsuka, T., Hata, Y., Ide, N., Yasuda, T., Inoue, E., Inoue, T., Mizoguchi, A., and Takai, Y. (1999). nRap GEP: a novel neural GDP/GTP exchange protein for rap1 small G protein that interacts with synaptic scaffolding molecule (S-SCAM). Biochem. Biophys. Res. Commun. *265*, 38–44.

Penzes, P., Johnson, R.C., Sattler, R., Zhang, X., Huganir, R.L., Kambampati, V., Mains, R.E., and Eipper, B.A. (2001). The Neuronal Rho-GEF Kalirin-7 Interacts with PDZ Domain–Containing Proteins and Regulates Dendritic Morphogenesis. Neuron *29*, 229–242.

Reedquist, K.A., Ross, E., Koop, E.A., Wolthuis, R.M., Zwartkruis, F.J., van Kooyk, Y., Salmon, M., Buckley, C.D., and Bos, J.L. (2000). The small GTPase, Rap1, mediates CD31-induced integrin adhesion. J. Cell Biol. *148*, 1151–1158.

Sala, C., Piech, V., Wilson, N.R., Passafaro, M., Liu, G., and Sheng, M. (2001). Regulation of dendritic spine morphology and synaptic function by Shank and Homer. Neuron, in press.

Sala, C., Rudolph-Correia, S., and Sheng, M. (2000). Developmentally regulated NMDA receptor-dependent dephosphorylation of cAMP response element-binding protein (CREB) in hippocampal neurons. J. Neurosci. *20*, 3529–3536.

Satoh, K., Yanai, H., Senda, T., Kohu, K., Nakamura, T., Okumura, N., Matsumine, A., Kobayashi, S., Toyoshima, K., and Akiyama, T. (1997). DAP-1, a novel protein that interacts with the guanylate kinase-like domains of hDLG and PSD-95. Genes Cells *2*, 415–424.

Scheffzek, K., Ahmadian, M.R., and Wittinghofer, A. (1998). GTPase-activating proteins: helping hands to complement an active site. Trends Biochem. Sci. *23*, 257–262.

Segal, M. (1995). Morphological alterations in dendritic spines of rat hippocampal neurons exposed to N-methyl-D-aspartate. Neurosci. Lett. *193*, 73–76.

Sheng, M., Cummings, J., Roldan, L.A., Jan, Y.N., and Jan, L.Y. (1994). Changing subunit composition of heteromeric NMDA receptors during development of rat cortex. Nature *368*, 144–147.

Sheng, M., and Pak, D.T.S. (2000). Ligand-gated ion channel interactions with cytoskeletal and signaling proteins. Annu. Rev. Physiol. *62*, 755–778.

Sorra, K.E., Fiala, J.C., and Harris, K.M. (1998). Critical assessment of the involvement of perforations, spinules, and spine branching in hippocampal synapse formation. J. Comp. Neurol. *398,* 225–240.

Takeuchi, M., Hata, Y., Hirao, K., Toyoda, A., Irie, M., and Takai, Y. (1997). SAPAPs, a family of PSD-95/SAP90-associated proteins localized at postsynaptic density. J. Biol. Chem. *272*, 11943–11951.

Toni, N., Buchs, P.A., Nikonenko, I., Bron, C.R., and Muller, D. (1999). LTP promotes formation of multiple spine synapses between a single axon terminal and a dendrite. Nature *402*, 421–425.

Torti, M., Bertoni, A., Canobbio, I., Sinigaglia, F., Lapetina, E.G., and Balduini, C. (1999). Interaction of the low-molecular-weight GTP-binding protein rap2 with the platelet cytoskeleton is mediated by direct binding to the actin filaments. J. Cell. Biochem. *75*, 675–685.

Tsukamoto, N., Hattori, M., Yang, H., Bos, J.L., and Minato, N. (1999). Rap1 GTPase-activating Protein SPA-1 Negatively Regulates Cell Adhesion. J. Biol. Chem. *26*, 18463–18469.

Vossler, M., Yao, H., York, R., Pan, M., Rim, C., and Stork, P. (1997). cAMP activates MAP kinase and Elk-1 through a B-Raf- and Rap1-dependent pathway. Cell *89*, 73–82.

Walikonis, R., Jensen, O., Mann, M., Provance, D.J., Mercer, J., and Kennedy, M. (2000). Identification of proteins in the postsynaptic density fraction by mass spectrometry. J. Neurosci. *20*, 4069–4080.

Wyszynski, M., Lin, J., Rao, A., Nigh, E., Beggs, A.H., Craig, A.M., and Sheng, M. (1997). Competitive binding of alpha-actinin and calmodulin to the NMDA receptor. Nature *385*, 439–442.

Xia, Z., Dudek, H., Miranti, C.K., and Greenberg, M.E. (1996). Calcium influx via the NMDA receptor induces immediate early gene transcription by a MAP kinase/ERK-dependent mechanism. J. Neurosci. *16*, 5425–5436.

Ziv, N.E., and Smith, S.J. (1996). Evidence for a role of dendritic filopodia in synaptogenesis and spine formation. Neuron *17*, 91–102.

Zwartkruis, F.J., and Bos, J.L. (1999). Ras and Rap1: two highly related small GTPases with distinct function. Exp. Cell Res. *253*, 157–165.

Zwartkruis, F.J., Wolthuis, R.M., Nabben, N.M., Franke, B., and Bos, J.L. (1998). Extracellular signal-related activation of rap1 fails to interfere in ras effector signaling. EMBO J. *17*, 5905–5912.